Copyright © 2005 American Scientific Publishers
All rights reserved
Printed in the United States of America

Journal of
Nanoscience and Nanotechnology
Vol. 5, 530–535, 2005

COMMUNICATION

Doping of Si into GaN Nanowires and Optical Properties of Resulting Composites

Congkang Xu,[1] Sangyong Chung,[1] Misuk Kim,[1] Dong Eon Kim,[1,*] Bonghwan Chon,[2] Sangsu Hong,[2] and Taiha Joo[2,*]

[1] Department of Physics and Electron Spin Science Center, [2] Department of Chemistry, Pohang University of Science and Technology, Pohang 790-784, South Korea

POSTECH (cid 35009164)
IP : 141.223.90.45
Sat, 04 Feb 2006 02:43:41

Doping of Si into GaN nanowires has been successfully attained via thermal evaporation in the presence of a suitable gas atmosphere. Analysis indicated that the Si-doped GaN nanowire is a single crystal with a hexagonal wurtzite structure, containing 2.2 atom % of Si. The broadening and the shift of Raman peak to lower frequency are observed, which may be attributed to surface disorder and various strengths of the stress. The band-gap emission (358 nm) of Si-doped GaN nanowires relative to that (370 nm) of GaN nanowires has an apparent blue shift (∼12 nm), which can be ascribed to doping impurity Si.

Keywords: GaN Nanowires, Raman Scattering, Photoluminescence, Nanocomposites.

AMERICAN SCIENTIFIC PUBLISHERS
Delivered by Ingenta to:

Recently, the fabrication and properties of nanometer-sized materials such as GaN nanowires (NWs) have attracted considerable attention owing to their potential applications in both testing the fundamental concept of quantum mechanics and the development of nanodevices.[1–5] So far, many techniques have been developed for the synthesis of pure GaN NWs such as laser ablation,[6,7] thermal chemical vapor deposition (CVD),[8–13] arc discharge,[14] nanotube-confined reaction,[15] and anodic alumina templates (AAO).[16] In order to exploit the practicable applications, it is of much importance and significance to tailor the properties of pure GaN NWs by doping special elements such as manganese, cobalt, and silicon. The former elements (Mn, Co) can introduce their magnetic properties to GaN NWs (diluted magnetic semiconductors); the latter may modify the conductivity and photoluminescence of GaN NWs. However, only a few experiments have been performed.[17,18] Theoretically, it has been reported that Si atoms residing in Ga sites in GaN are neutral shallow donors.[19] Thus, the Si-doped GaN nanowires are expected to have interesting electronic properties. This point attracts our scientific interest and is also needed for their future applications. Little work on doping of Si into GaN nanowires has been done to date; a simple and effective approach for the preparation of the nanowires remains a challenge. In this paper, we present single-crystalline Si-doped GaN nanowires and GaN nanowires via a simple route in the absence of template[17] and catalyst such as Au.[18] Si-doped GaN and undoped GaN NWs are synthesized through the reaction of high purity Ga_2O_3 powders with NH_3 and Ar 95% + H_2 5% in a furnace. The growth mechanisms of GaN based nanowires are discussed.

A quartz boat containing reagent-grade Ga_2O_3 powder (Aldrich, 99.99%) was kept in the center of a quartz tube placed horizontally in a tubular furnace as shown in Figure 1a. Cleaned SiO_2 substrates were placed downstream from the boat. The distances between the boat and substrates were 25 (A) and 30 cm (B), respectively. The base vacuum was kept at 95 mTorr. The powder was heated up to 900 °C at the rate of 15 °C/min with a flow of Ar 95% + H_2 5% at a rate of 60 sccm, Ar + H_2 gas was then turned off, and a pure ammonia gas (99.999%) was introduced at a rate of 150 sccm. The furnace was then heated up to 1080 °C at the rate of 10 °C/min and maintained for 160 min. The pressure was kept at 675 Torr. The temperature distribution is shown in Figure 1b. After the furnace was cooled with NH_3, the samples were taken from the substrates.

*Author to whom correspondence should be addressed.

 1533-4880/2005/5/530/006/$17.00+.25 doi:10.1166/jnn.2005.097

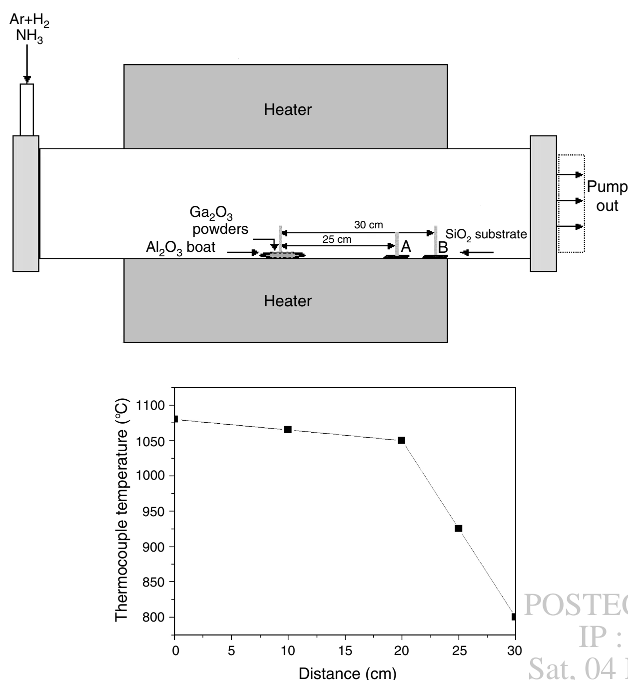

Fig. 1. (a) Schematic diagram of the horizontal furnace used in the synthesis. (b) The temperature distribution curve in the furnace.

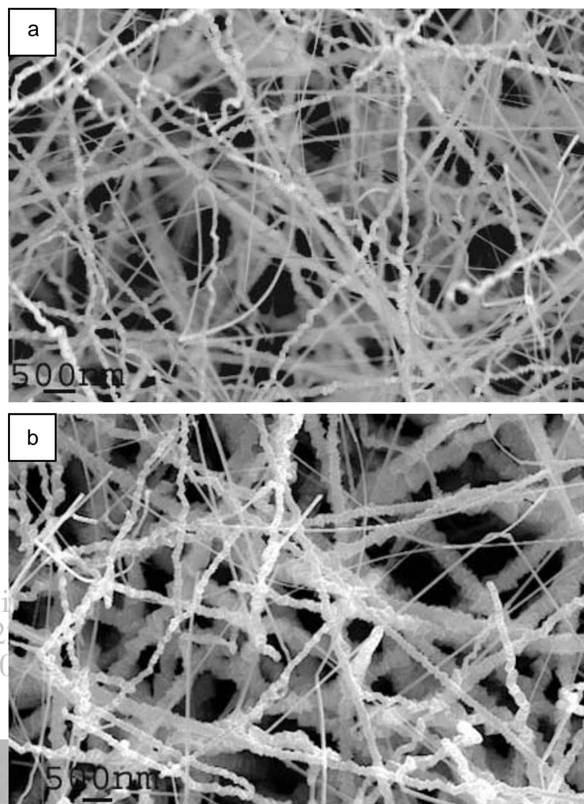

Fig. 2. Typical SEM images of the samples A (a) and B (b).

The as-prepared samples were investigated by X-ray diffraction (XRD, Rigaku D/max-rB Cu Kα). The morphology and size distribution of the nanowires were characterized with a scanning electron microscope (SEM, Hitachi H-8010) equipped with an energy-dispersive X-ray (EDX) spectroscometer and a transmission electron microscope (TEM, Hitachi H-800). High-resolution TEM (HRTEM), EDX and electron diffraction (ED) analysis were performed with JEOL-2010. The Raman backscattering measurements were performed at room temperature using a Spex 1403 Raman scattering spectrometer and a 200 mW Ar^+ laser at 488 nm as the excitation source. The third harmonic of a cavity-dumped femtosecond Ti:sapphire laser at 266 nm was used as an excitation source in the photoluminescence (PL) measurement.

Wool-like products on SiO_2 substrates appear in two distinguished colors. Typical SEM images of the sample A and B are shown in parts a and b of Figure 2, respectively. Sample A formed on substrate A at 25 cm (around 900–950 °C) downstream from the target materials is deep gray, whereas sample B formed on substrate B at 30 cm (around 800 °C) is light yellow. The boundary between these two regions was quite sharp. The diameters of the nanowires in sample A range from 50 to 200 nm, and the length is up to a few micrometers. The diameters of the nanowires in the sample B range from 50 to 450 nm. Statistic analyses indicate that the number of larger diameter nanowires in sample B is greater than that in sample A.

Figure 3 illustrates XRD of the as-prepared sample A and B. As shown in Fig. 3(a), the diffraction peaks in sample A are quite similar to those of a bulk GaN, which can be indexed to (100), (002), (101), (102), (110), (103), (200), (112), (201), and (004) of hexagonal wurtzite structure GaN ($a = 3.18$ Å, $c = 5.18$ Å). The diffraction data are in good agreement with published values[9] for GaN nanowires. No obvious diffraction peak corresponding to Si or Si compound impurity phases is observed. The peak (002) is the strongest, and other peaks are relatively weak. The strong intensities of the peaks relative to the background delineate that the nanowires are well-crystallized. However, the diffraction peaks of the sample B (Fig. 3b)

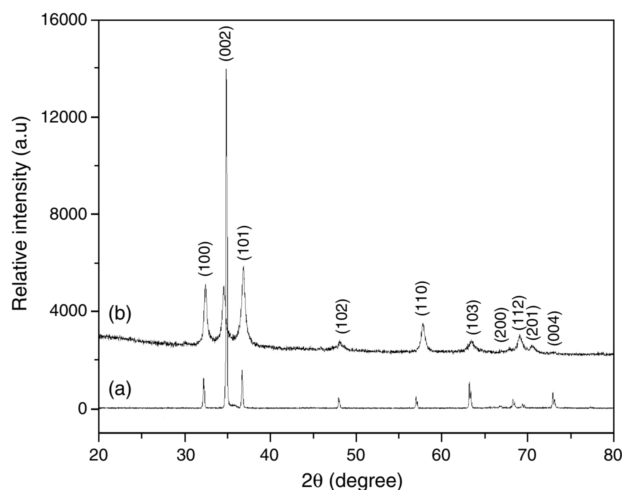

Fig. 3. XRD pattern of the as-prepared samples A (a) and B (b).

POSTECH (ci... IP : 141.2... Sat, 04 Feb 20... Delivered by Ingenta to: AMERICAN SCIENTIFIC PUBLISHERS

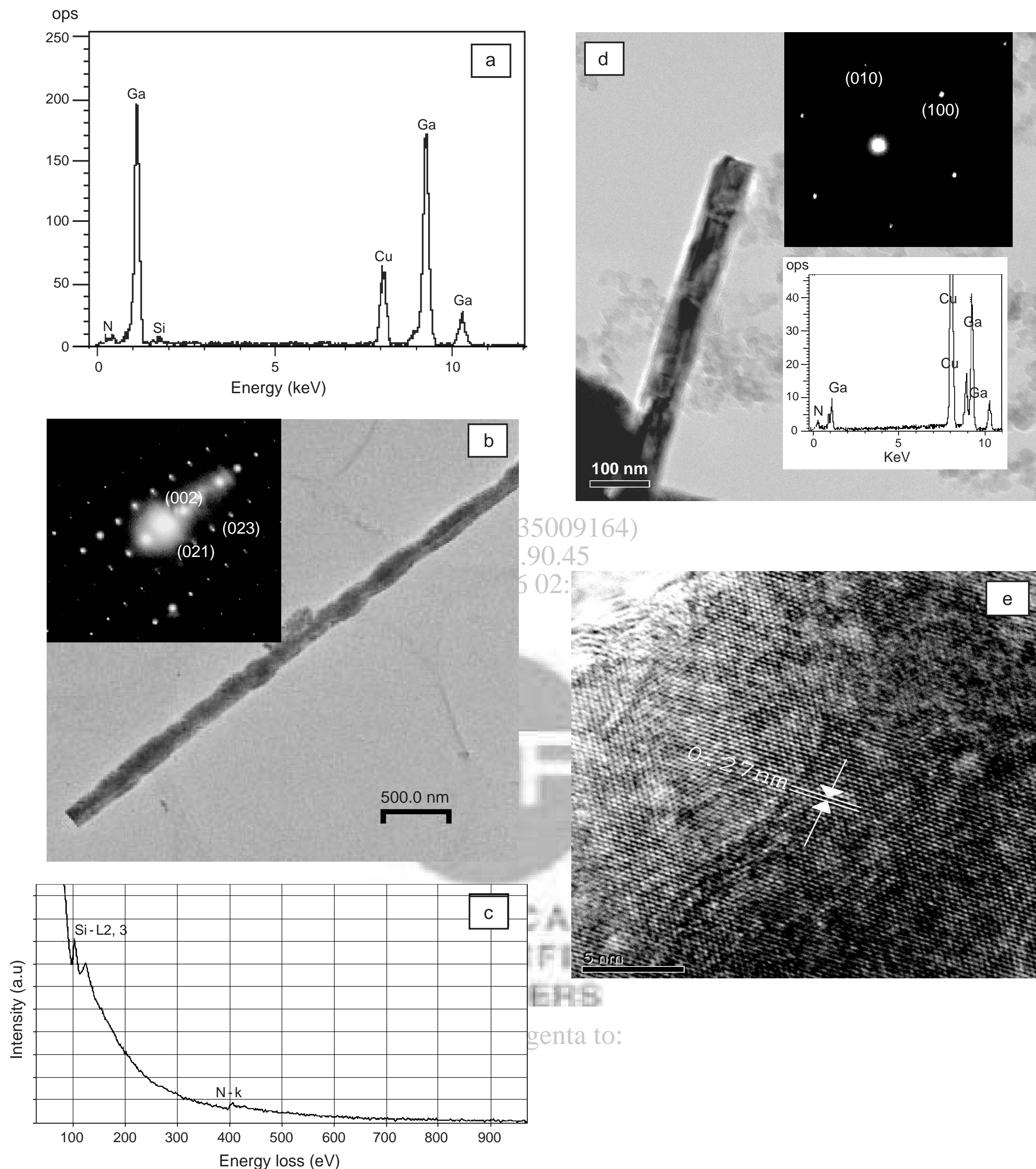

35009164)
.90.45
6 02:
genta to:

Fig. 4. (a) EDX of the sample A. (b) A typical TEM of the sample A, the inset is SAED. (c) EELS data of the nanowire grown on the substrate. (d) TEM image of the nanowire grown on the substrate B, the upper and lower insets are SAED and EDX, respectively. (e) HRTEM image of the nanowire in (d).

relative to the background are weaker, indicating that the crystallinity of sample B is not so good as that of sample A. In sample B, the peak (101) is the strongest, instead of (002).

Figure 4a shows the energy dispersive X-ray spectroscopy (EDX) analyses. It indicates that sample A consists of Ga, N, and Si, with an atomic ratio of 38.55 : 60.57 : 0.88. The atomic ratio of Ga to Si is about 97.8 : 2.2. Different areas of a single nanowire and dozens of nanowires have been analyzed by EDX attached to TEM. These results indicate that Si is uniformly contained in GaN nanowires. Figure 4b shows a typical bright-field TEM image of a nanowire. The inset is its selected area electron diffraction (SAED), which can be indexed to a wurtzite hexagonal structure GaN. This result indicates that the nanowire is a single crystal with [001] growth direction. In addition, no second set of diffraction points or irregular points was observed.

The electron energy loss spectra (EELS) data for a nanowire grown on substrate A is shown in Figure 4c.

The nanowire shows three distinct absorption features corresponding to Si–L_2, L_3, and N–K in the range of energy loss from 50 to 900 eV, indicating that Si has been doped into GaN nanowires.

Figure 4d shows a typical bright-field TEM image of the nanowire grown on the substrate B. The diameter of the nanowire is about 70 nm. The upper and lower insets are SAED pattern and EDX analysis, respectively. The EDX analysis indicates that the nanowire consists of Ga and N. The atomic ratio of Ga to N is about 49 : 51. The SAED pattern can be indexed to single-crystal hexagonal GaN; the [110] direction is parallel to the long axis of the nanowire, indicating that the fast-growth direction is along the [110] direction, which is different from the case of substrate A whose growth direction is along [001]. The lattice spacing of 0.27 nm, as shown in the HRTEM image (Fig. 4e), corresponds to (100) crystal planes of the hexagonal GaN.

There are probably several chemical reactions involved in our method to fabricate GaN based nanowires. According to the thermodynamic data, the Ga_2O_3 cannot directly react with NH_3 since the free energy of reaction is positive ($\Delta G_r = 180$–94 kJ/mol^{-1}) in the temperature range 300–1200 °C. Because of the presence of $Ar + H_2$, Ga_2O_3 will be reduced to Ga through the following reactions:[20]

$$Ga_2O_3(s) + 2H_2 \rightarrow Ga_2O(l) + 2H_2O(g) \quad (1)$$

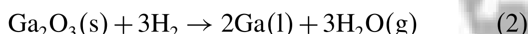

$$Ga_2O_3(s) + 3H_2 \rightarrow 2Ga(l) + 3H_2O(g) \quad (2)$$

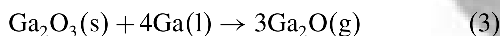

$$Ga_2O_3(s) + 4Ga(l) \rightarrow 3Ga_2O(g) \quad (3)$$

Moreover, NH_3 decomposes stepwise to NH_2, NH, H_2, and N_2 at temperature above 800 °C. Hence, H_2 can be assumed to be present in our furnace after the Ar + H_2 was turned off and NH_3 was introduced. As Ga_2O and Ga are much more volatile than Ga_2O_3 at the processing temperature, Ga can be readily transported to substrate A by the carrier gas. From a thermodynamic point of view, Ga can easily etch the surface of silica substrate around 950 °C. The following reaction may occur:[21]

$$4Ga(l) + SiO_2(s) \rightarrow 2Ga_2O(g) + Si(s) \quad (4)$$

Newly formed Si can dissolve into Ga to form Ga–Si droplets since Si cannot react with SiO_2 below 1100 °C.[22] The solubility of Si in Ga is about 5 atom % above 800 °C under vacuum.[23]

The following reaction occurs:

$$2Ga/Si + 2NH_3 \rightarrow 2GaN/Si + 3H_2 \quad (5)$$

$$Ga_2O(g) + 2NH_3(g) \rightarrow 2GaN + H_2O + 3H_2(g) \quad (6)$$

Reaction 6 might occur either in the vapor or in the Ga–Si droplets. The Ga_2O, NH_3, and GaN dissolve in the liquid alloy droplets of Ga–Si. When the GaN concentration reaches the saturation level in the Ga–Si droplet, solid GaN will segregate at the droplet–substrate interface. Thus, the Ga–Si droplet acts as a nucleation site for GaN segregation and as a medium to dissolve GaN and Si. Finally, $Ga_{1-x}Si_xN$ nanowires are formed.[18] In this process, the growth mechanism is dominated by vapor–liquid–solid (VLS).[21]

Because the temperature of the substrate A (900–950 °C) is a bit less than the decomposition temperature (above 950 °C) of GaN,[24,25] some GaN based nanowires are more likely to be unstable and subsequently decompose into Ga and N_2:

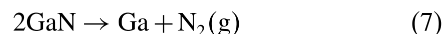

$$2GaN \rightarrow Ga + N_2(g) \quad (7)$$

Si(s) segregates from Ga. Ga will be carried away by carrier gas and deposited onto substrate B (around 800 °C). From a thermodynamic point of view, reaction 4 is not workable, since the temperature of substrate B is below 900 °C. No silicon source is available. Hence, the following reaction occurs:

$$2Ga(g) + 2NH_3(g) \rightarrow 2GaN(s) + 3H_2(g) \quad (8)$$

In this reaction, partial Ga is probably from reaction 2.

$$Ga_2O(g) + 2NH_3(g) \rightarrow 2GaN + H_2O + 3H_2(g) \quad (9)$$

In this process, the growth mechanism is likely to be governed by vapor solid (VS).

Raman scattering is sensitive to microscopic structure, which can provide further information on vibrational states of $Ga_{1-x}Si_xN$ and GaN nanowires. On the other hand, according to band mode and the selection rules, we can also judge its crystalline quality. In terms of the factor group analysis, a single-crystal GaN possesses eight sets of optical phonon modes near the zone center. These modes are classified into Raman ($A_1 + E_1 + 2E_2$), silent ($2B_1$), and infrared active ($A_1 + E_1$). The A_1 and E_1 modes are further split into LO (longitudinal optical) and TO (transverse optical) components. For the sample A, as shown in Figure 5a, first, the four observed Raman-active phonon bands near 136, 527, 563, and 703 cm^{-1} correspond to E_2 (low), A_1 (TO), E_2 (high), and A_1 (LO) modes, respectively. The frequencies of the first three modes are close to those previously reported on nanowires and bulks;[26–28] the position of the A_1 (LO) mode is significantly softer. Second, we find that these phonon peaks broaden substantially in the case of the nanowires. Third, the strongest E_2 (high) phonon line reflects the characteristics of the hexagonal crystal phase of the GaN nanowires. Only the allowed modes according to the selected rule are manifested, illustrating that structural defects or internal stress are minimal in the sample. Two additional modes were observed at 419 and 665 cm^{-1}, both of which are not allowed by the C_{6v} space group in first-order Raman scattering at the zone center. The peak at 419 cm^{-1} can

POSTECH (cid 35000161)
IP: 141.223.90.45
Sat, 04 Feb 2006 02:43:41
AMERICAN SCIENTIFIC PUBLISHERS
Delivered by Ingenta to:

COMMUNICATION

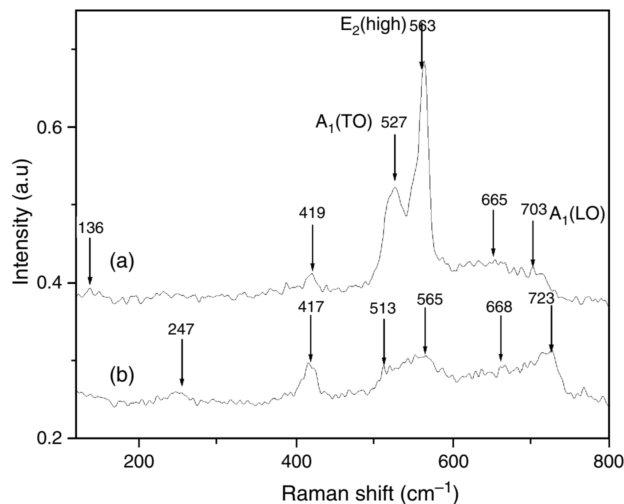

Fig. 5. Raman scattering spectroscopy of the samples A (a) and B (b).

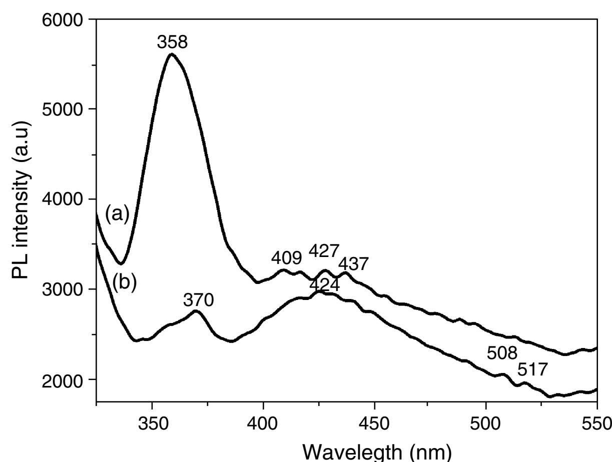

Fig. 6. PL spectra of the samples A (a) and B (b).

COMMUNICATION

be assigned to the zone-boundary phonon, whereas the peak at 665 cm^{-1} can be indexed into the defect-induced phonon mode. This behavior agrees with the spatial correlation or phonon confinement model, which suggests that phonons in nanometric systems can be confined in space by crystallite boundaries or surface disorders. Consequently, this confinement causes an uncertainty in the wave vector of the phonons, which results in broadening of the Raman features. Similar evidence for the broadening of the Raman bands associated with the phonon confinement effects has been observed in the micro- and nanocrystallite systems, such as Si and GaAs.[29]

For the sample B, as shown in Figure 5b, the peaks at 513, 565, and 723 cm^{-1} are the first-order phonon frequencies of A_1(TO), E_2(high), and A_1(LO), respectively.[9] The strength of A_1(LO) is almost the same as that of E_2(high), that is, $I_{E_2(\text{high})}/I_{A_1(\text{LO})} \leq 1$, which is contrary to the common observation of a high $I_{E_2(\text{high})}/I_{A_1(\text{LO})}$ ratio. This may be assigned to surface disorder and strong stress in the differently oriented unit cells along the growth.

Apparently, the peaks of both sample A and B were shifted to lower frequency and broadened compared to those of bulk GaN single crystal.[30–32] The red shifts of the E_2(high), A_1(LO), and A_1(TO) modes are 3, 23, and 5 cm^{-1}, respectively. Gao et al.[33] also found a red shift in the Raman scattering spectrum of Ga_2O_3 nanorods, in the present work; because gallium oxide was used as a starting material and residual oxygen existed in the furnace, the gallium oxide is probably incorporated into GaN nanowires. Accordingly, we also believe that the red shift of GaN nanowires originated from some defects and further investigation is needed.

Figure 6 shows the room temperature (300 K) PL spectra of the Si-doped GaN (Fig. 6a) and undoped GaN nanowires (Fig. 6b). A band-edge emission was observed at 358 nm (3.46 eV) for the $Ga_{1-x}Si_xN$. The well-known defect-induced yellow emission band is not observed, indicating high quality of the Si-doped GaN nanowires. A broad emission band around 425 nm (2.92 eV) was also observed, which should be related with defect sites and/or surface states. In PL spectra of GaN doped with Mn or Mg, similar bands at 425 nm (2.92 eV) have been observed,[34,35] indicating that this band may arise from the defect sites. For GaN nanowires, band-edge emission was observed at 370 nm (3.37 eV) with much weaker intensity, whereas the 425-nm (2.92 eV) emission becomes much stronger, indicating that defect concentration is higher in the GaN nanowire.

The band-edge emission of the Si-doped GaN nanowire is blue-shifted from that of the GaN nanowires by ∼12 nm (∼90 meV). Although a significant fraction of the Si-doped GaN nanowires have diameters less than that of GaN, quantum confinement may not be responsible for the blue shift, since the diameters of the nanowires are much larger than the exciton Bohr radius of the bulk GaN (2.8 nm). The blue shift may also arise from the Si dopant. Recent research on Si-doped GaN film has attributed the shift of the band gap to the shifts of both conduction and valence bands.[36] The band-edge emission showed non-monotonic behavior: the position decreases initially as the dopant concentration increases and showed an increase by further increase in doping. A more detailed PL study is in progress and will be published in a separate paper.

In summary, a bulk quantity of Si-doped GaN and undoped GaN nanowires has been successfully synthesized via conventional CVD method in the presence of a suitable gas atmosphere. Several techniques were employed to analyze the as-prepared nanowires, indicating that the Si-doped GaN nanowires have a single-crystal hexagonal wurtzite structure along with 2.2 atom % Si. The broadening and the lower frequency shift of Raman peaks are probably attributed to surface disorder and the stress. The blue shift of band-gap emission of Si-doped GaN nanowires relative to that of GaN nanowires is due to doping impurity Si.

POSTECH (cid 35009161) IP: 141.223.90.45 Sat, 04 Feb 2006 02:13:41 Delivered by Ingenta to: AMERICAN SCIENTIFIC PUBLISHERS

Acknowledgments: This project was supported in part by the electron Spin Science Center (eSSC) funded by Korea Science and Engineering foundation (KOSEF) and BK 21 project in 2004 funded by Korea Research foundation.

References and Notes

1. G. Fasol, *Science* 272, 1751 (**1996**).
2. S. Nakamura, *Science* 281, 956 (**1998**).
3. H. Morkoc and S. N. Mohanmmad, *Science* 267, 51 (**1995**).
4. W. Han, S. Fan, Q. Li, and Y. Hu, *Science* 277, 1287 (**1997**).
5. F. A. Ponce and D. P. Bour, *Nature* 386, 351 (**1997**).
6. W. Shi, Y. Zheng, N. Wang, C. Lee, and S. Lee, *Adv. Mater.* 13, 591 (**2001**).
7. X. Duan and C. Lieber, *J. Am. Chem. Soc.* 122, 188 (**2000**).
8. C. Chen and C. Yeh, *Adv. Mater.* 12, 738 (**2000**).
9. M. He, I. Minus, P. Zhou, S. Mohammed, J. Halpern, R. Jacobs, W. Sarney, L. Salamanca-Riba, and R. Vispute, *Appl. Phys. Lett.* 77, 3731 (**2000**).
10. C. C. Chen, C. H. Yeh, C. H. Chen, M. Yu, H. Liu, J. Wu, K. H. Chen, L. C. Chen, J. Peng, and Y. F. Chen, *J. Am. Chem. Soc.* 123, 2791 (**2001**).
11. X. Chen, J. Li, Y. Cao, Y. Lan, H. Li, M. He, C. Wang, Z. Zhang, and Z. Qiao, *Adv. Mater.* 12, 1432 (**2000**).
12. J. R. Kim, H. So, J. Park, J. J. Kim, J. Kim, C. Lee, and S. Lyu, *Appl. Phys. Lett.* 80, 3548 (**2002**).
13. K. Chang and J. Wu, *J. Phys. Chem. B* 106, 7796 (**2002**).
14. W. Han, P. Redlich, F. Ernst, and M. Rühle, *Appl. Phys. Lett.* 76, 652 (**2000**).
15. W. Han, S. Fan, Q. Li, and Y. Hu, *Science* 277, 1287 (**1997**).
16. G. Chen, L. Zhang, Y. Zhu, G. Fei, L. Li, C. Mo, and Y. Mao, *Appl. Phys. Lett.* 75, 2455 (**1999**).
17. F. L. Deepak, P. V. Vanitha, A. Govindaraj, and C. N. R. Rao, *Chem. Phys. Lett.* 374, 314 (**2003**).
18. J. Liu, X. M. Meng, Y. Jiang, C. S. Lee, I. Bello, and S. T. Lee *Appl. Phys. Lett.* 83, 4241 (**2003**).
19. J. Neugebauer and C. G. van de Walle, *Phys. Rev. B* 57, 2033 (**1998**).
20. Z. Lan, C. Liang, C. Hsu, C. Wu, H. Lin, S. Dhara, K. Chen, L. Chen, and C. Chen, *Adv. Funct. Mater.* 14, 233 (**2004**).
21. C. C. Tang, S. S. Fan, M. L. Chapelle, and P. Li, *Chem. Phys. Lett.* 333, 12 (**2001**).
22. R. B. Heslop and P. L. Robinson, *Inorganic Chemistry*, Elsevier, New York (**1960**), p. 287.
23. B. Girault, F. Chevrier, A. Joullie, and G. Bougnot, *J. Cryst. Growth* 37, 169 (**1977**).
24. H. W. Choi, M. A. Rana, S. J. Chua, T. Osipowicz, and J. S. Pan, *Semicond. Sci. Technol.* 17, 1223 (**2002**).
25. J. Y. Li, X. L. Chen, Z. Y. Qiao, Y. G. Cao, and Y. C. Lan, *J. Cryst. Growth* 213, 408 (**2000**).
26. T. Azuhata, T. Sota, K. Suzuki, and S. Nakamura, *J. Phys.: Condens. Matter.* 7, L129 (**1995**).
27. L. Filippidis, H. Siegle, A. Hoffmann, C. Thomsen, K. Karch, and F. Bechstedt, *Phys. Status Solidi B* 198, 621 (**1996**).
28. V. Y. Davydov, Y. E. Kitaev, I. N. Goncharuk, A. N. Smirnov, J. Graul, O. Semchinova, D. Uffmann, M. B. Smirnov, A. P. Mirgorodsky, and R. A. Evarestov, *Phys. Rev. B* 58, 12 899 (**1998**).
29. X. S. Zhao, Y. R. Ge, J. Schroeder, and P. D. Persans, *Appl. Phys. Lett.* 65, 2033 (**1994**).
30. W. J. Wang, Y. T. Song, W. X. Yuan, Y. G. Cao, X. Wu, and X. L. Chen, *Appl. Phys. A* 78, 29 (**2004**).
31. G. Wei, J. Zi, K. Zhang, and X. Xie, *J. Appl. Phys.* 82, 4693 (**1997**).
32. Y. G. Cao, X. L. Chen, Y. C. Lan, Y. P. Xu, T. Xu, and J. K. Ling, *J. Mater. Res.* 15, 267 (**2000**).
33. Y. H. Gao, Y. Bando, T. Sato, and Y. F. Zhang, *Appl. Phys. Lett.* 81, 2267 (**2002**).
34. M. Leroux, N. Grandjean, B. Beaumont, G. Nataf, F. Semond, J. Massies, and P. Gibart, *J. Appl. Phys.* 86, 3721 (**1999**).
35. J. M. Baik, J. L. Lee, Y. Shon, and T. W. Kang, *J. Appl. Phys.* 93, 9024 (**2003**).
36. A. F. D. Silva, C. M. Araujo, B. E. Sernelius, and C. Persson, *J. Phys.: Condens. Matter.* 13, 8891 (**2001**).

Received: 27 August 2004. Revised/Accepted: 16 November 2004.

POSTECH (cid 35009164)
IP : 141.223.90.45
Sat, 04 Feb 2006 02:43:41
AMERICAN SCIENTIFIC PUBLISHERS
Delivered by Ingenta to: